LA-3478, Part I

c. 3

LOS ALAMOS SCIENTIFIC LABORATORY
of the
University of California
LOS ALAMOS • NEW MEXICO

Time-of-Flight Neutron Cross-Section Measurements Made with Neutrons from Nuclear Explosions

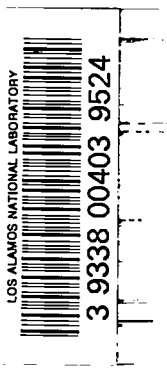

UNITED STATES
ATOMIC ENERGY COMMISSION
CONTRACT W-7405-ENG. 36

This report expresses the opinions of the author or authors and does not necessarily reflect the opinions or views of the Los Alamos Scientific Laboratory.

Printed in the United States of America. Available from Clearinghouse for Federal Scientific and Technical Information National Bureau of Standards, U. S. Department of Commerce Springfield, Virginia 22151

Price: Printed Copy $3.00; Microfiche $0.65

LA-3478, Part I
UC-34, PHYSICS
TID-4500

LOS ALAMOS SCIENTIFIC LABORATORY
of the
University of California
LOS ALAMOS • NEW MEXICO

Report written: December 10, 1967

Report distributed: June 18, 1968

Time-of-Flight Neutron Cross-Section Measurements Made with Neutrons from Nuclear Explosions

by

A. Hemmendinger
B. C. Diven
W. K. Brown
A. Ellis
A. Furnish
E. R. Shunk
R. R. Fullwood

TIME-OF-FLIGHT NEUTRON CROSS-SECTION MEASUREMENTS MADE WITH NEUTRONS FROM NUCLEAR EXPLOSIONS

by

A. Hemmendinger, B. C. Diven, W. K. Brown, A. Ellis

A. Furnish, E. R. Shunk, and R. R. Fullwood

ABSTRACT

Well-known laboratory techniques have been adapted to meet the specific requirements of neutron time-of-flight measurements using as a source the neutrons emitted in a nuclear detonation. The experimental arrangements and hardware are described, with particular attention to parameters affecting neutron flux and energy resolution. Details of instrumentation and data recording schemes are presented.

I. INTRODUCTION

The principle of identifying a nuclear event by measuring its neutron energy in terms of transit time over a known distance was first applied in a laboratory experiment by Dunning et al.[1] With the advent of more intense pulsed sources, faster electronics, and multichannel recording schemes, this method has been highly developed.[2] Nevertheless, the rate at which high resolution cross-section measurements can be made is limited by the strength of laboratory neutron sources, and for measurements on highly radioactive nuclides the rate of emission of laboratory sources presents a further limitation; even years of continuous running would not produce good data. It has long been tempting to use the neutrons generated in a nuclear detonation for time-of-flight measurements; in the last few years the means of using these very intense sources have been at hand.

A relatively small nuclear yield, say one kiloton of TNT equivalent, releases 10^{23} neutrons in a burst lasting 0.1 μsec. Many years of continuous accelerator operation would be required to produce an equal number of neutrons, and the emission rate

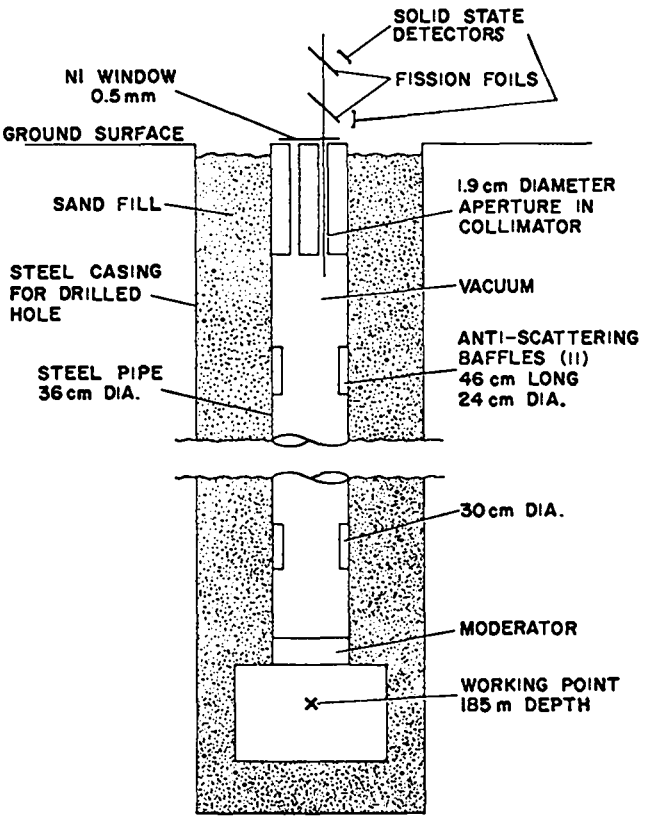

Fig. 1. Line-of-sight pipe to provide vacuum flight path for neutrons originating in a nuclear explosion.

of an accelerator source during a single pulse is lower by a factor of 10^{10}.

The kind of hardware that might be used for collimation of neutrons from a nuclear detonation is shown schematically in Fig. 1. An evacuated steel pipe, 36-cm o.d., with many anti-scattering baffles, provides a flight path for neutrons. A collimator can provide several beams, and an array of experiments can be stacked in each beam. A tower centered over the line of sight (see Fig. 2) has been used to accommodate many different experiments. The use of catchers to stop neutron beams that have served their purpose, and of extensive shielding between floors of the tower, minimizes cross talk between experiments.

After an underground explosion deep in the desert alluvium, there is ground subsidence which subjects equipment over the hole to free fall of from 15 to 60 ft. This fall, which is much more destructive than the ground shock from the explosion, wrecks the tower and much of the tower-borne equipment. The use of a sled pulled by a winch has proved quite successful in recovery of equipment before cratering occurs. Sleds can also be pulled down a ramp from the first floor of a tower as shown in Fig. 3. One sled carrying a reaction chamber and preamplifiers has been used in three different exposures, and is now being refurbished for a fourth.

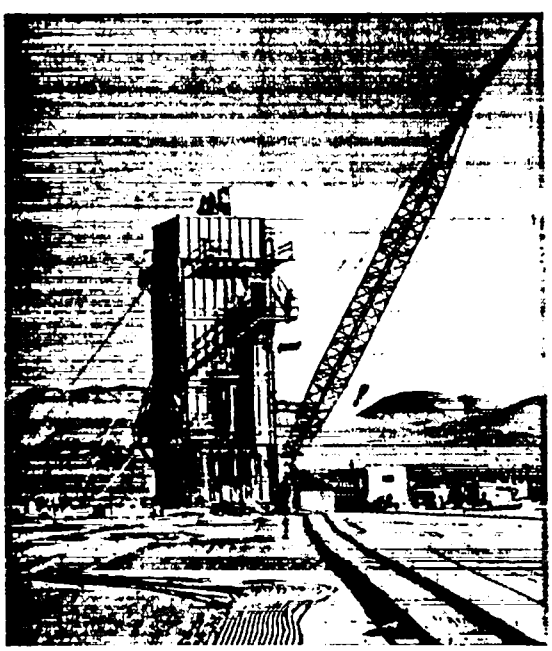

Fig. 2. Tower centered over the line of sight.

A time-of-flight neutron experiment using one intense burst of neutrons is characterized by reaction rates much too great to allow counting of single events. Instead, we must use a counting rate meter, the output of which is recorded as a function of time. In doing this we give up the possibility of pulse-height analysis or of coincidence counting. Against these two disadvantages are balanced the advantages of very great neutron flux in a parallel beam: short-lived nuclides can be used as targets, backgrounds that would be prohibitive in the laboratory become negligible, and many very thin targets can be stacked to give ratios of cross sections over an energy range of 10 to 10^7 eV, eliminating the many normalizations and changes in target or equipment required in laboratory experiments.

To produce enough good measurements to justify the effort of a field experiment, we also require: (1) fast logarithmic amplifiers to record many decades of signal current on (typically) the 0-to 15-V range of an oscilloscope, and (2) a scheme for recording these amplifier outputs over a span of many milliseconds with 0.1-μsec resolution.

Historically, the first experiment in which we were sure that we could distinguish between signal and background was done at the Nevada Test Site of the U. S. Atomic Energy Commission on an explosion code-named Pipefish on April 29, 1964. On Parrot, December 16, 1964, a full-fledged experiment showed the possibility of making good cross-section measurements,[3,4] although the instrumentation used was still not quite adequate. On Petrel, June 11, 1965, fission cross-section measurements were made on ^{239}Pu, ^{240}Pu, ^{241}Pu, ^{233}U, ^{235}U, ^{241}Am, and $^{242}Am^{m}$, and capture cross sections on ^{240}Pu and ^{238}U. These have been reported in detail,[5-10] and are a significant contribution to compiled fission data.[11] On Persimmon, February 23, 1967, data were acquired by various groups at Los Alamos, with collaboration of Idaho Nuclear Corporation and AWRE, Aldermaston, on fission of ^{238}Pu and ^{244}Cm, and capture of ^{238}Pu, ^{147}Pm, ^{151}Eu, ^{153}Eu, ^{175}Lu, and ^{93}Nb, all of which are expected to yield good cross sections.

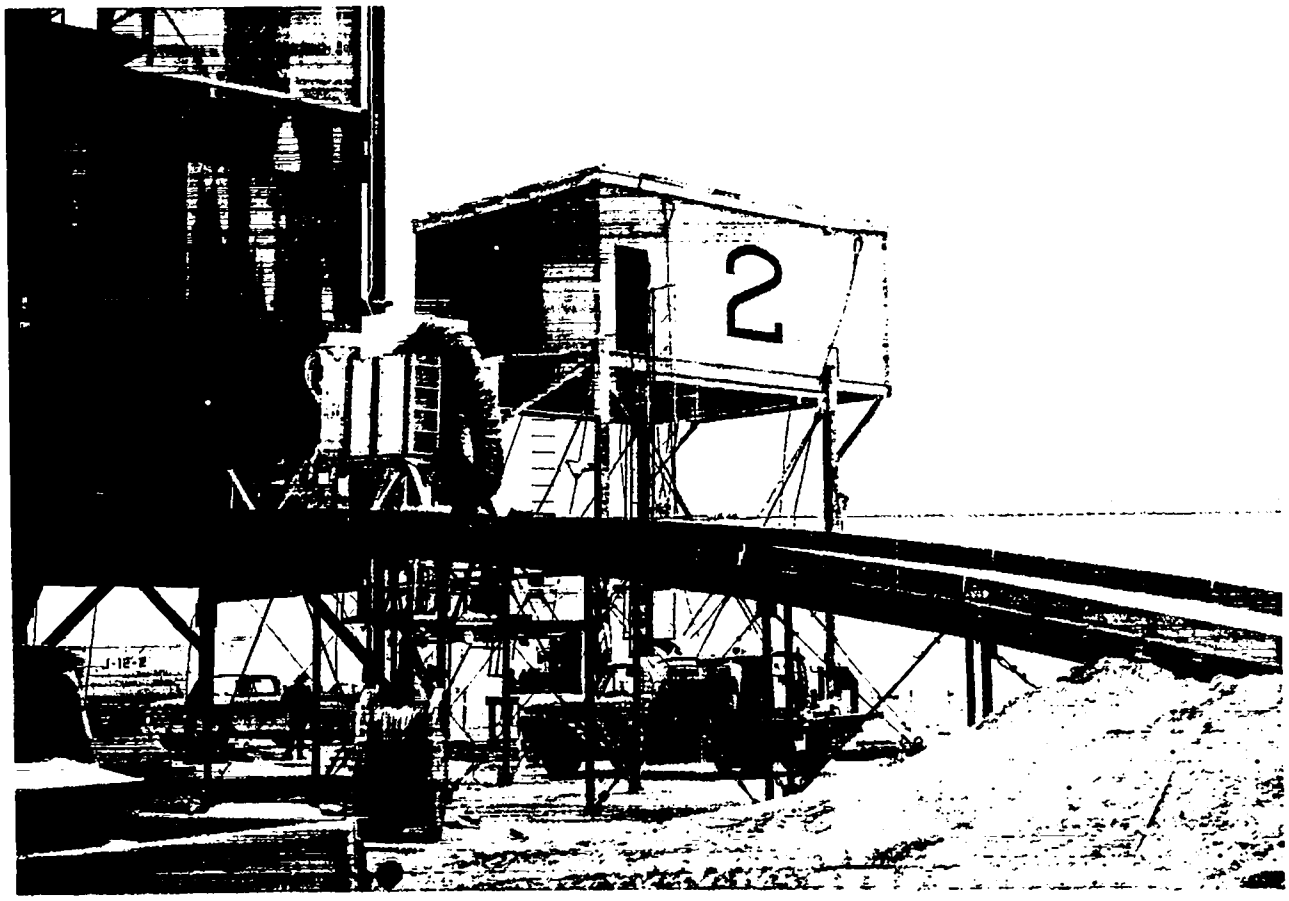

Fig. 3. Sled pulled from the first floor of the tower.

II. THE NEUTRON BEAM

The determination of a minimum safe burial depth for containment of an underground detonation has been the subject of extensive study. We will assume a depth, typical for Los Alamos field operations, of

$$\ell = 122\ Y^{1/3} \text{ meters}, \tag{1}$$

with the bomb yield, Y, in kilotons.

The neutron yield depends on design details, but a typical yield is 10^{23} neutrons/kt. If, for neutron energy, E, we denote by S(E) the number of neutrons per unit energy interval leaving the source, the number emerging from aperture A of a collimator at ground surface is

$$n(E) = \frac{A}{4\pi\ell^2}\, S(E). \tag{2}$$

If t is the neutron flight time in microseconds,

$$E = 5227\ell^2 t^{-2} \text{ eV}, \tag{3}$$

$$t = 72.30\ \ell E^{-\frac{1}{2}}, \tag{4}$$

and the energy spread for a source pulsed for Δt microseconds is

$$\Delta E = -0.0277E^{3/2}\ \frac{\Delta t}{\ell} \text{ eV}. \tag{5}$$

The neutron current through the collimator is

$$I(t) = \frac{A\ S(E)}{4\pi\ell^2}\ \frac{dE}{dt} \tag{6}$$

$$= \frac{EAS(E)}{2\pi\ell^2 t}\ . \tag{7}$$

Substituting t from Eq. 4 in Eq. 7, we get

$$I(E) = \frac{0.002186\ A\ S(E)E^{3/2}}{\ell^3}\ . \tag{8}$$

If we use a flight path defined by Eq. 1,

$$I(E) = \frac{9.292 \times 10^{-10} A\ S(E)E^{3/2}}{Y}, \tag{9}$$

and the energy resolution given by Eq. 5 becomes

$$\frac{\Delta E}{E} = \frac{2.27 \times 10^{-4} E^{\frac{1}{2}}\ \Delta t}{Y^{1/3}}\ . \tag{10}$$

We see from Eq. 9 that for the flight path of Eq. 1 the neutron current is independent of the yield (because S is proportional to Y), and from Eq. 10 that the energy resolution improves as $Y^{1/3}$.

A development of major significance has been the insertion of a "cold" moderator into the flight path above the bomb source. This modifies the neutron spectrum, typically transferring neutrons down to lower energy regions[12] where there would otherwise be a shortage. One of our experiments (Parrot) had no moderator; another (Petrel) used a 5-cm-thick polyethylene moderator, shielded from gamma-ray heating by a lead slab. The beam spectra in these two experiments are shown in Fig. 4 for comparison. Within limits, and depending on how much resolution we can afford to sacrifice, the spectrum can be adjusted. Normally we seek a spectrum that minimizes the dynamic range of the signals.

The rate of a reaction in a target is

$$R(t) = I(t)\rho_A\sigma(E), \qquad (11)$$

where $\sigma(E)$ is the cross section for the reaction and ρ_A is the atomic density of the target in atoms per unit projection of the target area along the beam direction. The target material, on a foil, is arranged to cover the intersection of the beam and the foil. Note that if the spectrum of neutrons can be tailored by a moderator to approximate an E^{-1} shape, and if σ is proportional to v^{-1}, then the reaction rate becomes

$$R(t) \propto S(E)\frac{dE}{dt}\sigma(E) = \text{constant}. \qquad (12)$$

This constant R(t) is ideal for precision of recorded data.

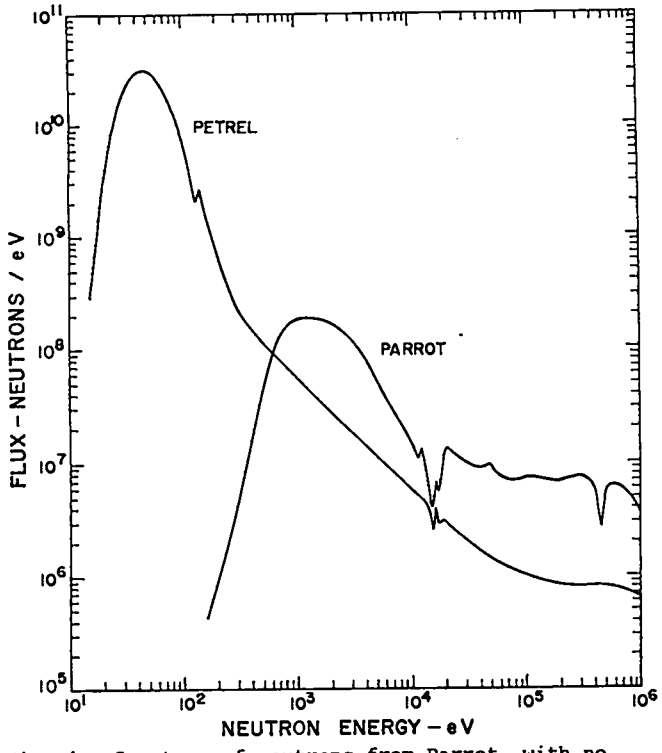

Fig. 4. Spectrum of neutrons from Parrot, with no moderator, and Petrel, with 5 cm of polyethylene.

A theoretical derivation of the neutron spectrum can be made;[13] but is not needed here. For visualization, the source S(E), can be separated into these categories:

$S_1(E)$ neutrons from nuclear reactions, including fission,

$S_2(E)$ neutrons scattered by, and moderated in, hot hydrogenous materials around a bomb,

$S_3(E)$ neutrons from a cold moderator, scattered and slowed to the actual temperature of the moderator.

As $S_1(E)$ and $S_2(E)$ feed each other, and both feed $S_3(E)$, it is not easy to relate them absolutely to the observed beam spectrum.

A significant feature at the extreme low energy end of the spectrum is the "cut off" caused by the motion of the cold moderator which is driven upward in the beam direction by the explosion. The moderator overtakes and removes neutrons with velocities less than its own.

Collimator tubes 4 to 6 ft long were made of alternate sections of brass and steel. Monel tubes have also been used. Beam purity, in time-of-flight context, is the degree of freedom from contamination by "wrong time" neutrons in the beam at the point of measurement. Inelastic scattering in the pipe walls is a credible source of such neutrons. Anti-scattering baffles are designed to keep these neutrons from reaching the collimator aperture. That excellent beam purity is obtained is demonstrated by the presence of deep valleys between resonances in the data. The background is, in fact, as low as that obtainable in measurements using accelerators. Contamination of the beam with gamma radiation is negligible, as gamma production ends along with the neutron burst. The gamma flash may, however, be responsible for the large background, present on all signals, that decays with a time constant of

perhaps 6 or 7 μsec. This background is removed in data processing by subtracting measurements made at the same time using blank sample foils.

At high energies, all neutrons originate at a short distance, ℓ, from the center of the bomb. At lower energies neutrons diffuse, first from a hot moderator, then from a cooler moderator. Each moderator is at a distance less than ℓ, so there are, in effect, small shifts in the time scale.

A sharp resonance is broadened by Doppler motion of the target atoms, giving a full width at half-maximum of

$$\Delta E = 4(EkT\ \ell n2)^{\frac{1}{2}} \left(\frac{m}{M}\right)^{\frac{1}{2}}, \qquad (13)$$

where E is neutron energy; k, Boltzmann's constant; T, the effective temperature; m, the neutron mass; and M, the target nuclide mass.

Contributions of target nuclide motion and burst duration to the energy resolution are plotted in Fig. 5. Because Doppler broadening dominates at low energies, there seems little point to using flight paths longer than 200 m in this range. At the higher energies, where the resolution is determined by $\Delta t/\ell$, longer flight paths give better energy resolution.

III. APPARATUS

Detectors were arrayed on the surface of a sphere, with the fission foil centered in the equatorial plane. The neutron beam intersected the foil at the center of the sphere at an angle of 45°. The target geometry is simple if the neutron beam is uniform, the areal density of the target is constant, and the beam passes through the center of the foil; otherwise a more detailed analysis is required. Figure 6 shows the geometric relations required for a general treatment of the problem. To find the average solid angle subtended by the detector at the target we must know the beam density as a function of position on the foil, which can be determined by an autoradiograph of an activated foil, and the areal

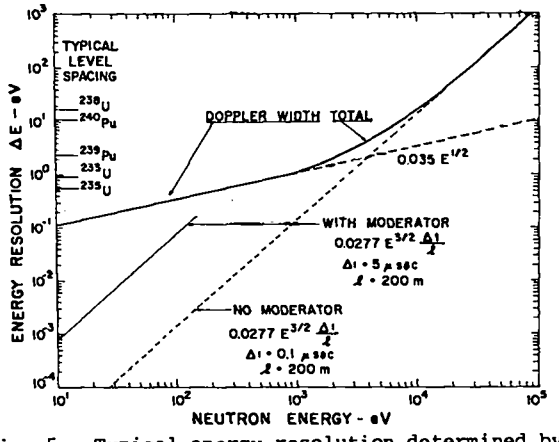

Fig. 5. Typical energy resolution determined by the Doppler effect (0.035 $E^{\frac{1}{2}}$, from Eq. 13) at low energies, burst duration (Eq. 5) of 0.1 μsec at high energies, and moderated burst duration of 5 μsec at low energies. Some typical level spacings of heavy nuclides are indicated.

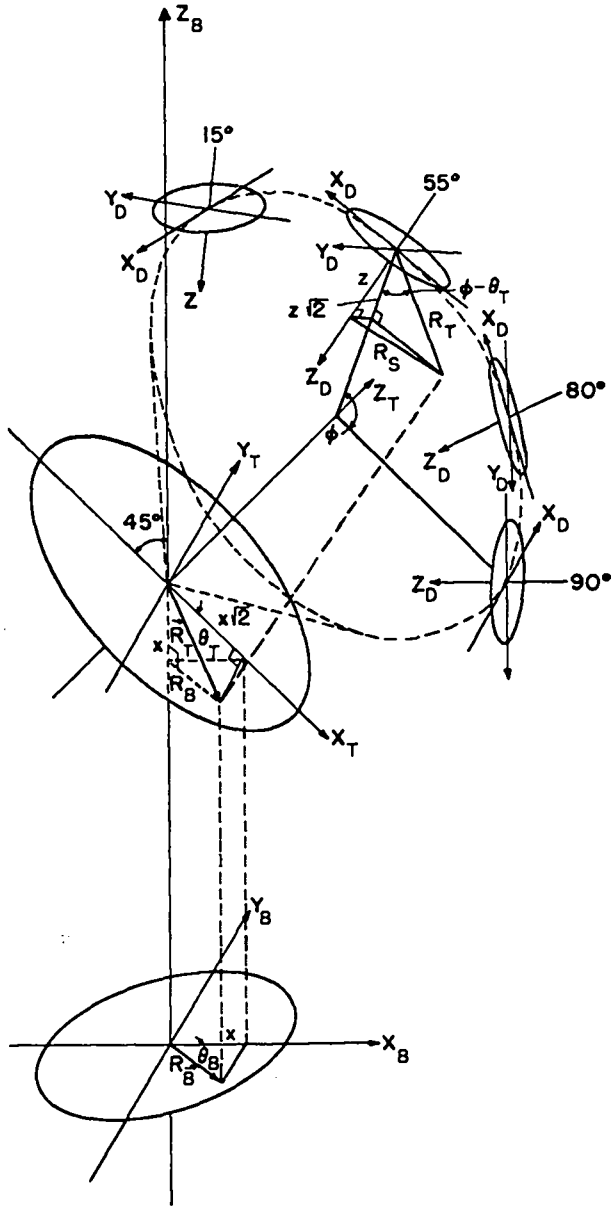

Fig. 6. Beam-target-detector geometry. Each detector axis is inclined at 45° to the target plane, forming a cone with axis Z_T and apex angle 90°. The target plane is inclined at 45° to the beam axis Z_B. All coordinate systems are right-handed.

density of the target, which in some cases can be determined by scanning the target with a telescope sensitive to the target's spontaneous disintegration products. If we let R_D be the radius of the detector, Z_O be the distance from detector center to target center, and θ_L be the laboratory angle of the detector, then, referring to Fig. 6 we see that

$$R_T^2 = R_B^2 (1+\cos^2\theta_B) \tag{14}$$

$$\text{or } \cos\theta_T = \cos\theta_B \sqrt{\frac{2}{1+\cos^2\theta_B}} ; \tag{15}$$

this gives the projection R_T on the foil of a radius vector R_B with polar angle θ_B. Furthermore, from Fig. 6,

$$z = \sqrt{\frac{1}{2}}\, R_T \cos(\theta_T-\phi) , \tag{16}$$

$$R_S^2 = R_T^2-z^2 = R_T^2[1-\tfrac{1}{2}\cos^2(\theta_T-\phi)] , \tag{17}$$

and

$$Z_S = Z_O-z = Z_O-\frac{1}{\sqrt{2}} R_T \cos(\theta_T-\phi) \tag{18}$$

where ϕ = angle in target plane of the projection of the $-Z_D$ axis,

$\cos\phi = 1-2\cos\theta_L$,

$\phi > 0$ for right side detectors,

$\phi < 0$ for left side detectors (not shown in Fig. 6).

The solid angle subtended at the source point in the foil by the detector is

$$\Omega(R_S,Z_S) = \int \frac{dA_\perp}{d^2} \tag{19}$$

$$= 2Z_S \int_o^\pi \int_o^{R_D} \frac{r\,dr\,d\theta}{(r^2-2rR_S\cos\theta+R_S^2+Z_S)^{3/2}} . \tag{20}$$

If we designate by $f_B(R_B,\theta_B)$ the beam density, and by $f_T(R_T,\theta_T)$ the target areal density, then the average solid angle, suitably weighted by these two functions, is

$$\Omega(R_D,Z_O,\theta_L) = \frac{\int_o^{2\pi}\int_o^{\infty} f_B(R_B,\theta_B) f_T(R_T,\theta_T) \Omega(R_S Z_S) R_B dR_B d\theta_B}{\int_o^{2\pi}\int_o^{\infty} f_B(R_B,\theta_B) f_T(R_T,\theta_T) R_B dR_B d\theta_B} \tag{21}$$

Mountings were interchangeable; a pair of cross hairs on the foil mounting permitted telescopic alignment with the thumbscrews shown in Fig. 7. Also shown in Fig. 7 is a camera shutter that limits to about one second the period of irradiation of the

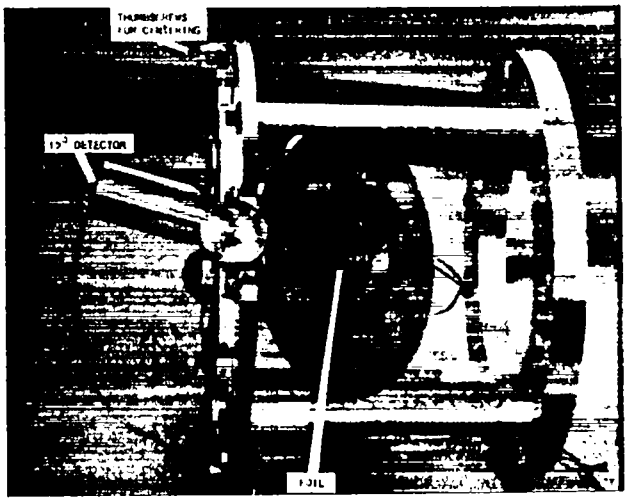

Fig. 7. Module for mounting one foil and its detectors.

detectors by alpha particles from the foil.

The signal from a detector located at an angle (θ_L) with respect to the neutron beam gives the differential cross section $\sigma(\theta_L)$ for a nuclear reaction. We usually want to find the reaction cross section, which is the integral of the differential cross section over all solid angles. Data reduction is simplified by letting all charged particles traverse the same thickness of target material; it is this requirement that makes Fig. 6 look so complicated.

For the measurement of capture cross sections, the charged particle detector was replaced by one sensitive to gamma rays but relatively insensitive to scattered neutrons, such as that devised by Moxon and Rae[14] in which a converter of gamma rays to electrons was mounted in front of a thin scintillator. In an adaptation[15] for these experiments the scintillator was replaced by a solid-state detector; in this form the gamma-ray detector has lower sensitivity to neutrons than the original version of Moxon and Rae which was not convenient for neutrons above 200 keV because proton recoils were counted in the scintillator.

Total cross sections may be measured by standard beam attenuation methods with flux-measuring detectors in the beam above and below the sample. The measurement of scattering cross sections is also feasible, but they are generally more difficult because they demand a detector with high efficiency

for scattered neutrons, low efficiency for gamma rays, and short resolving time.

Several methods have been used for mounting fission samples. The samples have been deposited by an evaporation process (^{235}U, ^{239}Pu) or painted on a backing and heated in air to form an oxide (^{242}Am, ^{241}Am). The heat to which the foil backing is subjected during the vaporization process or the heating cycle determines the method suitable for mounting the foil backings. For depositing some samples the foil backings are subjected less than 250°C, and for other samples to more than 700°C. For T < 250°C the foil backing can be glued or soft-soldered to a support ring.

The soft-solder method is preferred since it is easy and produces a very taut foil backing provided, of course, that the coefficient of thermal expansion of the foil is somewhat greater than that of the support ring. For soft-soldering backings of either nickel or platinum the support ring can be made of invar.

For T > 250°C two methods have been used to fabricate foil backings: silver-soldering the foil to a support ring or clamping it between two support rings. At silver-soldering temperatures the coefficient of thermal expansion of invar overtakes that of nickel and platinum, so an invar support ring is not suitable. The only successful silver-soldered backings (those used on Petrel) were made using 0.5-mil platinum foil and molybedenum support rings. On Persimmon, 0.25-mil platinum foil soft-soldered to invar or silver-soldered to molybdenum rings provided the backing for all fission samples.

The stack of detector modules shown in Fig. 8 was mounted in a vacuum chamber, which in turn was mounted on a sled (Fig. 9) along with logarithmic preamplifiers, vacuum pumps, voltage regulators, and air conditioners. The box containing the preamplifiers was protected from ground shock by surrounding it on all six sides by inner tubes inflated to 3 lb/in^2.

IV. ELECTRONIC INSTRUMENTATION

Most of the components used to produce and record data in these field experiments are standard, commercially available items. Figure 10 shows the

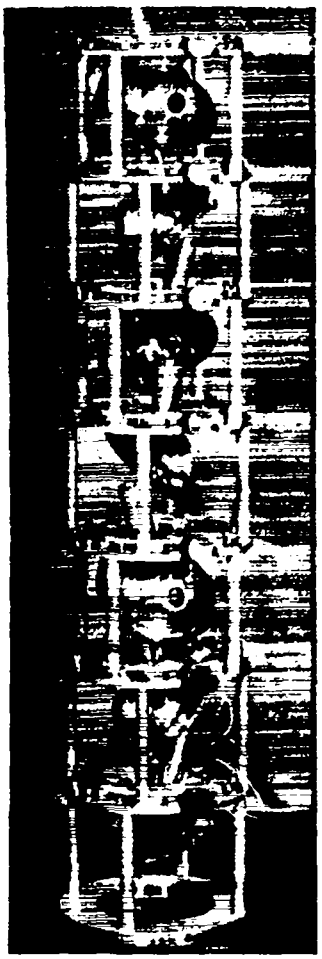

Fig. 8. A detector stack made up from modules.

essential features of a single-channel system. Not indicated are the various circuits for:

1. Starting 35-mm cameras early enough so they are at proper speed at zero time;
2. Intensifying the electron beams in oscilloscopes;
3. Turning on a calibrating pulser after the neutron signal has been recorded.

The recording stations used so far have been 15 x 35 ft frame buildings, well reinforced, with an aluminum skin for shielding. The buildings were floated on a layer of inflated truck tires placed on the deck of a skid. In this configuration the shock mounts customarily used for electronic equipment did more harm than good, and present practice is to bolt all electronic racks securely to the building. A typical distance from recording station to the hole for the nuclear explosive is 1000 ft.

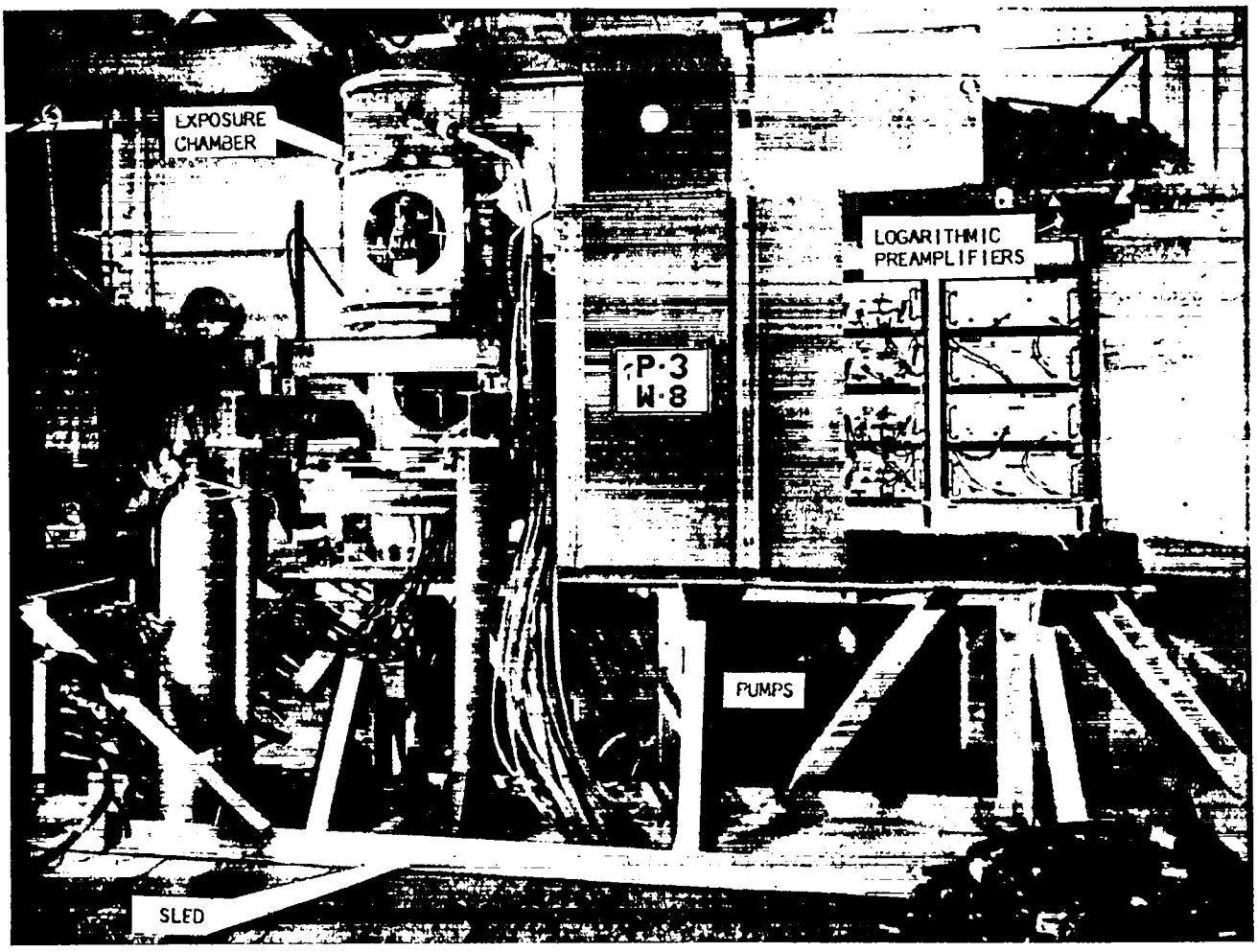

Fig. 9. Sled carrying chamber for exposing samples, logarithmic preamplifiers, pumps, and voltage regulators.

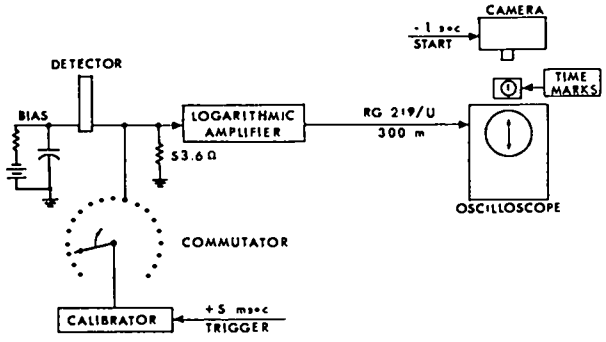

Fig. 10. Schematic showing one detector, log preamplifier, cable, calibrator, and recorder.

To date no equipment inside a recording station has been damaged by ground shock.

Detectors

Of the various known methods of detecting charged particles, solid-state detectors have been most attractive because of their speed and simplicity. Of all the detectors considered, thin-window, fully depleted, diffused-junction p-n diodes appeared most practical.[15] These detectors have a collection time of a few nanoseconds; linear response when exposed to short, intense, bursts of ionizing particles; and stability over long periods.

Logarithmic Preamplifiers

The four-decade logarithmic preamplifiers used in early experiments[16] have been modified by addition of another decade, by reducing undershoot following a large short pulse, and decreasing the sensitivity to negative signals in noise pickup. The current log preamplifier circuit (Model 6) is shown schematically in Fig. 11. Figure 12 shows an input-

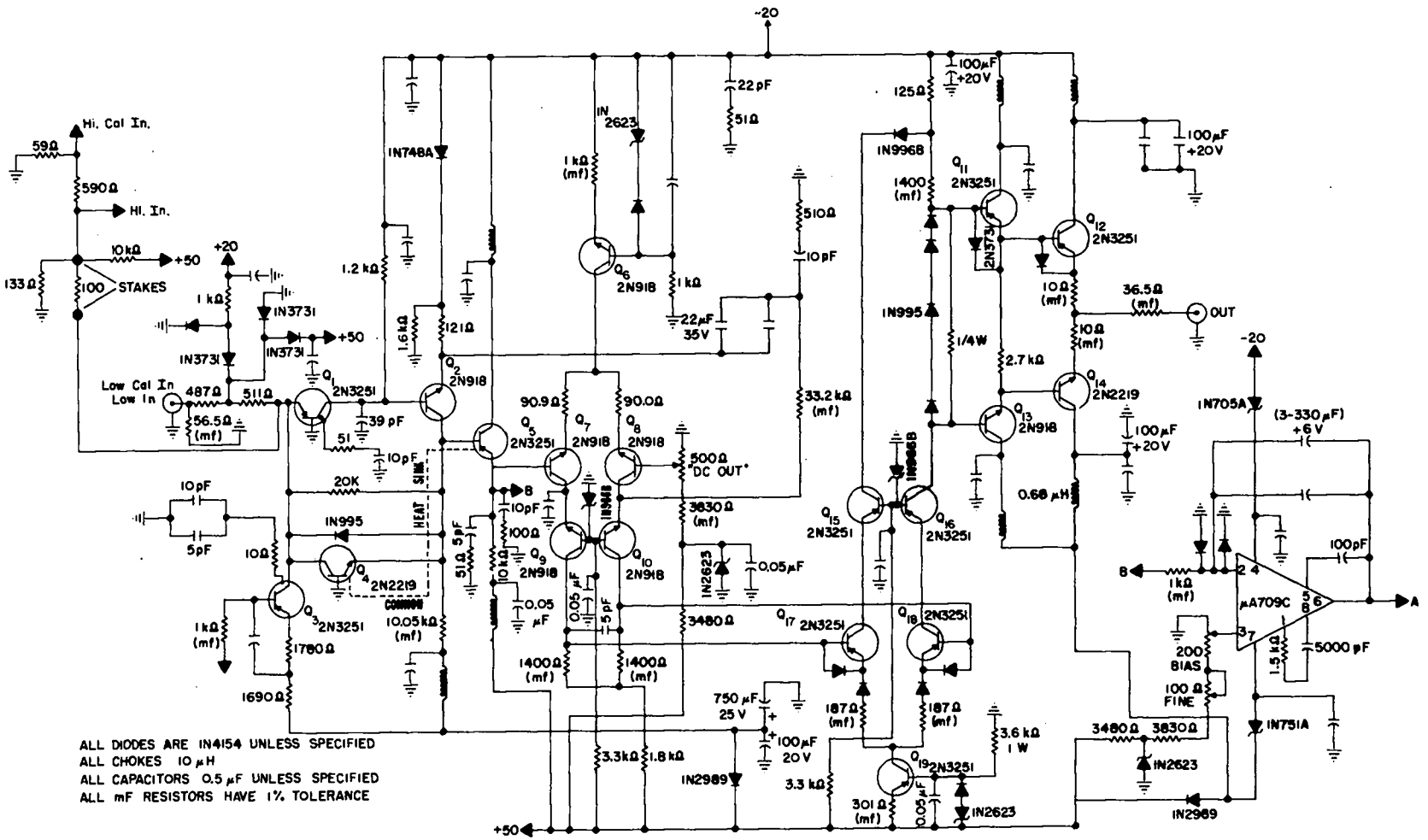

Fig. 11. LASL Model 6 logarithmic preamplifier.

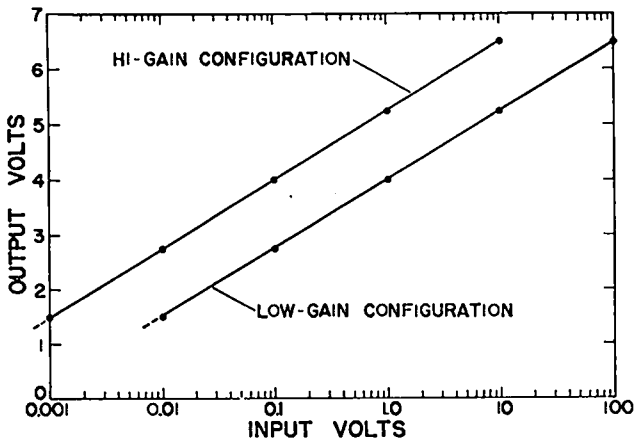

Fig. 12. LASL Model 6 logarithmic preamplifier, input-output characteristic.

output characteristic. The preamplifier is changed from high-gain to low-gain configuration by simple changes in the input network.

Amplitude Calibration

Amplitude calibration for each signal record is provided by impressing a stair-step voltage at the input of the logarithmic preamplifier, with the steps adjusted to span the dynamic range of the preamplifier in nearly equal steps as shown in Fig. 13. The ground loops that result from connecting the preamplifier inputs in parallel can be avoided by using double-pole commutation so that the calibrating pulser is connected to each preamplifier in sequence. Banks of magnetic reed switches have been used for commutation, with the reeds actuated by spinning magnets or, preferably, by a set of solenoids driven by a ring of multivibrators, shown in Fig. 14.

The LASL Model 3A stair-step calibrator, shown schematically in Fig. 15 has an input trigger signal to start the calibration signal, a synchronized output trigger, and an output signal.

Data Distortion by Cable Transmission

The analog signals originating at the exposure chamber must be transmitted a distance of 1000 ft or more. The distortions associated with this transmission can be classified as due to cable characteristics and the admixing of extraneous signals.

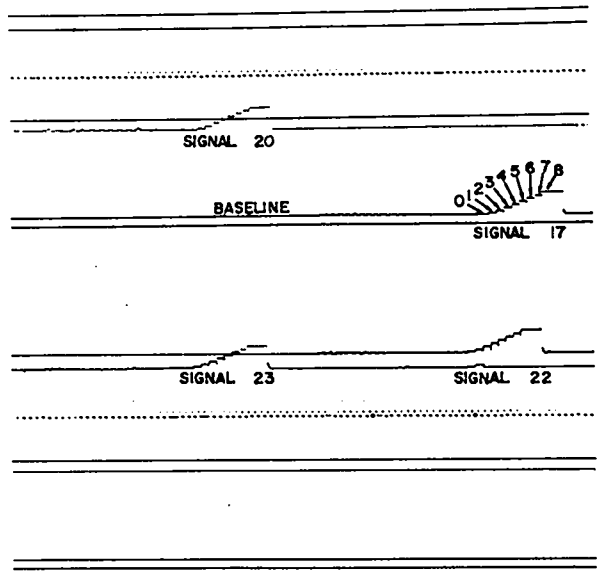

Fig. 13. Calibration signals at output of logarithmic preamplifier, displayed along with five other signals and a set of time marks.

Signal Distortion due to Cable Characteristics

Signal transmission has been by coaxial cables operating in the fundamental mode. Coaxial cables differ from other waveguide structures in that the lowest frequency in the pass band is zero. This has the distinct advantage that it is not necessary to modulate a carrier with the signal to be transmitted, a process that can introduce complexity and inaccuracy. It would be possible, however, to transmit all the signals over a single waveguide instead of the 50 or so coaxial cables. Some authors[17] have suggested this microwave carrier technique for avoiding unwanted signal pickup, but there are no known instances of its use.

A transmission line may be viewed as a filter with a finite transit time. To transmit a pulse without distortion, the attenuation, α, as a function of frequency, ω, must be constant and the delay in the cable must be constant for all frequencies.[18] Stated in another way, the phase shift is proportional to frequency. As a practical matter, to transmit a pulse of duration T it is necessary to satisfy the previous conditions only up to frequencies 2/T. The amplitude of frequencies above this contributes little. (Reference 18, p. 59.) Conversely, if a step function is applied to a cable (or a low pass filter), the minimum length of the

square pulse it will pass without distortion is about twice this rise time.

For cables whose attenuation is primarily due to the skin effect in the conductors, the first-order response has been obtained by Wigington and Nahman.[19] They find the response to a δ function to be of the form

$$g(t) = \frac{1}{\tau}\frac{1}{\sqrt{\pi}}\left(\frac{\tau}{t}\right)^{3/2} e^{-\tau/t} \qquad (22)$$

where

$$\tau(\text{nsec}) = \frac{10.12 \times 10^{-5}\xi^2 L^2}{F(\text{Mc})} \qquad (23)$$

F is the frequency at which the attenuation ξ in db per 100 ft is measured, and L is the cable length in feet.

The function g(t) is Poissonian-looking and has a long tail. The fraction of the peak value at long times is

$$\varepsilon_g = 2.43\left(\frac{\tau}{t}\right)^{3/2} \quad t >> \tau \qquad (24)$$

The response to a step function is obtained by convolution with g(t); it is

$$h(t) = 1\text{-erf}\left(\frac{\sqrt{\tau}}{t}\right), \qquad (25)$$

where erf(x), the error integral, is tabulated.[20]

h(t) looks like a rounded step very slowly approaching the asymptotic value. Using a power series representation of erf $\left(\frac{\sqrt{\tau}}{t}\right)$, the asymptotic dependence is obtained. The error by which the function h(t) differs from its asymptotic value of one at long times is

$$\varepsilon_h = \frac{2}{\sqrt{\pi}}\sqrt{\frac{\tau}{t}} \quad t >> \tau. \qquad (26)$$

A more relistic case than either of the previous is the response to a rectangular pulse of unit amplitude and duration T for the practical case $T >> \tau$.

The solution is obtained by combining positive and negative step functions displaced in time by T, as indicated in Fig. 16.

The solution is

$$p(t) = 0 \qquad \tau < 0,$$

$$= 1\text{-erf}\left(\sqrt{\frac{\tau}{t}}\right) \quad 0 < \tau < T,$$

$$= \text{erf}\left(\sqrt{\frac{\tau}{t-T}}\right) - \text{erf}\left(\sqrt{\frac{\tau}{t}}\right) \quad \tau > T. \qquad (27)$$

The peak value of p(t) will be the value at $t = T$ which is

$$p_{max}(T) = 1 - \text{erf}\left(\sqrt{\frac{\tau}{T}}\right). \qquad (28)$$

The fractional error by which this peak value fails to reach the value of the input pulse is obtained by a power series expansion for the case $T >> \tau$,

$$\varepsilon_p^{\text{peak}} = \frac{2}{\sqrt{\pi}}\sqrt{\frac{\tau}{T}}. \qquad (29)$$

The error relative to the peak input value by which the cable fails to return to the baseline is obtained by a power series expansion of p( ); it is

$$\varepsilon_p^{\text{return}} = -\frac{1}{\sqrt{\pi}}\frac{T}{\tau}\sqrt{\frac{\tau}{t}} \quad t >> T >> \tau. \qquad (30)$$

The negative sign indicates an undershoot.

As an example, τ for 1000 ft of RG 219 coaxial cable is 0.2 nsec. So, after 2.54 μsec the error in the measurement of the peak is 1%, and after 0.1 μsec it is 5%. If the pulse were 0.1-μsec wide, then after 1 μsec the undershoot would be 0.08%.

Table I lists pulse parameters for commonly used 50-ohm cables. The parameters were evaluated at 10 MHz for all cables. When several types of cables are used to transmit a signal, a composite τ,

$$\tau_{comp} = \left(\sum_{i=1}^{n} \tau_i^2\right)^{1/2},$$

is used where τ_i is the value of τ for each cable separately. Table II lists cable response to delta-function and step-function excitations.

Robert C. Perisho has written a program called CABLE which will predict signal distortion for more realistic input functions. These are introduced in the form of a subroutine, and at present include rectangular, Gaussian, and Breit-Wigner single-level pulses.

Signal Distortion by Noise Pickup

Because of the many unknown quantities, a complete mathematical analysis of the problems of electrical shielding is not useful. Instead, certain principles and the effectiveness of using magnetically loaded cables will be developed.

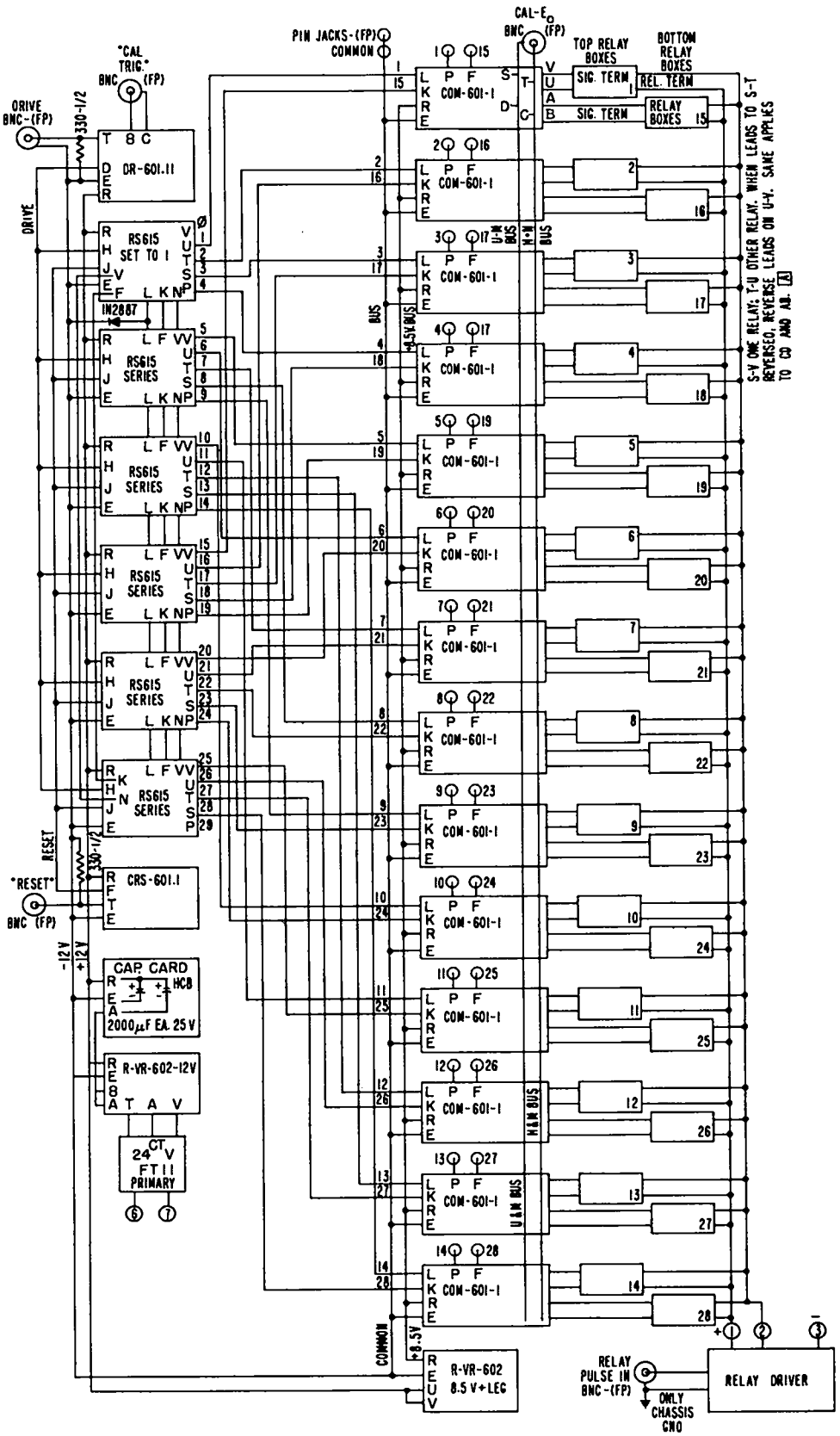

Fig. 14. Circuitry for commutation of preamplifier inputs so that calibration signals are applied

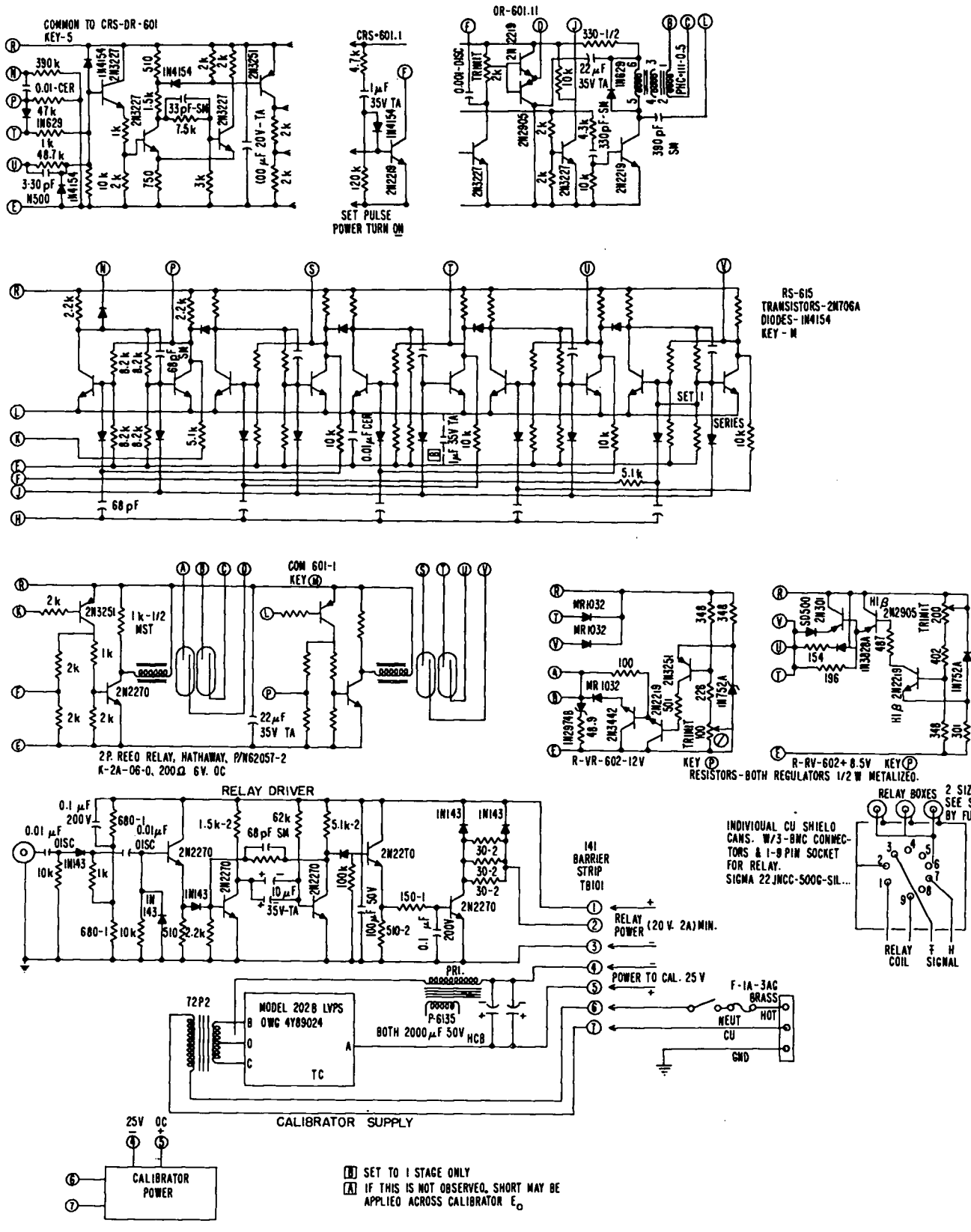

sequentially to one preamplifier at a time.

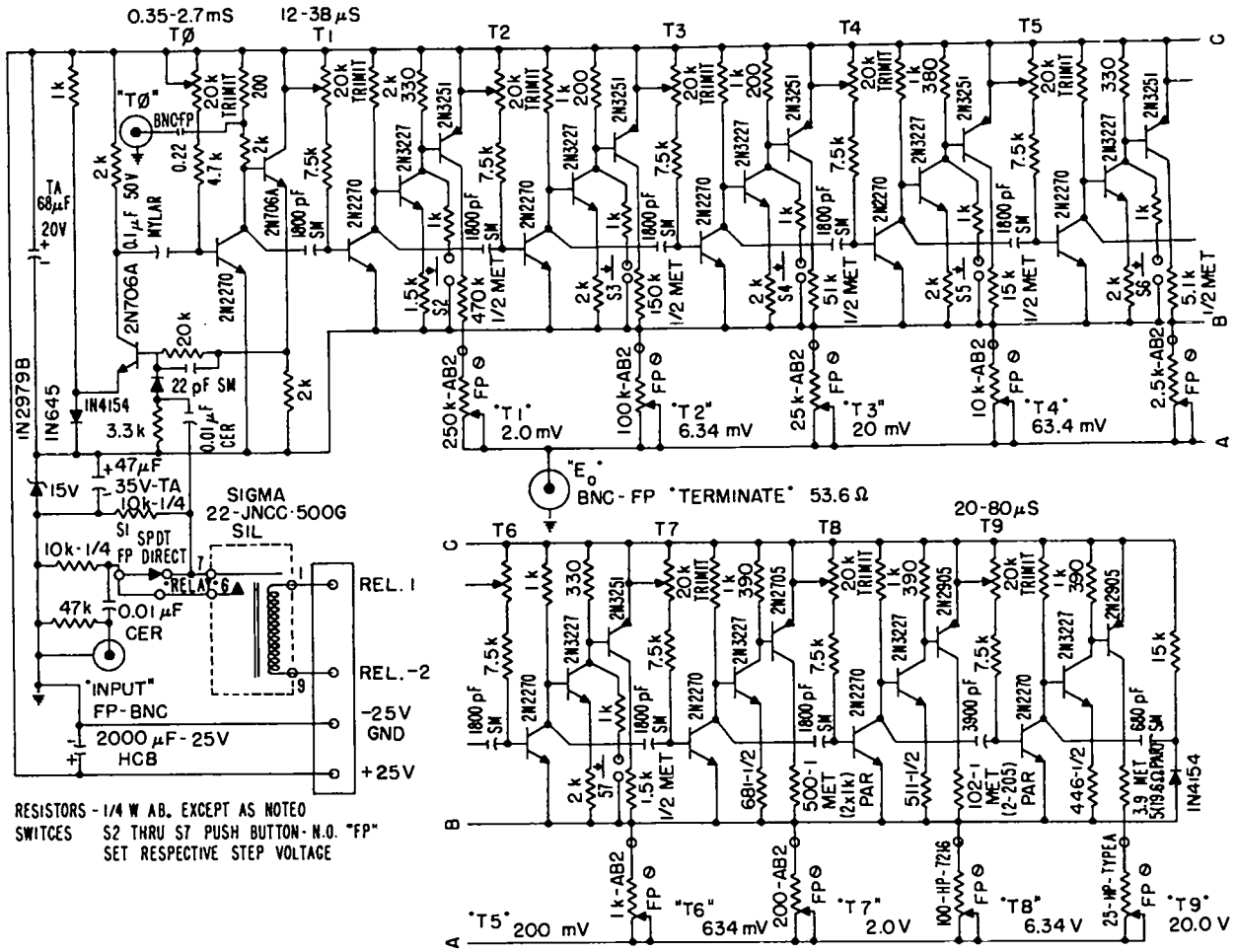

Fig. 15. LASL Model 3A stair-step calibrator.

Table I. Pulse Parameters for Commonly Used 50-Ohm Coaxial Cables at 10 MHz

Response	Microdot 3804	RG 58A	RG 55, 223	RG 8, 213, 215	RG 17, 18 177, 218, 219	3/8-in. Foam Flex
τ(nsec) for 1 ft	2.5×10^{-4}	2.7×10^{-5}	1.7×10^{-5}	3.0×10^{-6}	5.8×10^{-7}	6.3×10^{-7}
τ(nsec) for 10 ft	2.5×10^{-2}	2.7×10^{-3}	1.7×10^{-3}	3.0×10^{-4}	5.8×10^{-5}	6.3×10^{-5}
τ(nsec) for 50 ft	0.63	6.8×10^{-2}	4.3×10^{-2}	7.5×10^{-3}	1.5×10^{-3}	1.6×10^{-3}
τ(nsec) for 100 ft	2.5	0.27	0.17	3.0×10^{-2}	5.8×10^{-3}	6.3×10^{-3}
τ(nsec) for 500 ft	6.3	6.8	4.3	0.75	0.15	0.16
τ(nsec) for 1000 ft	250.	27.	17.	3.0	0.58	0.63

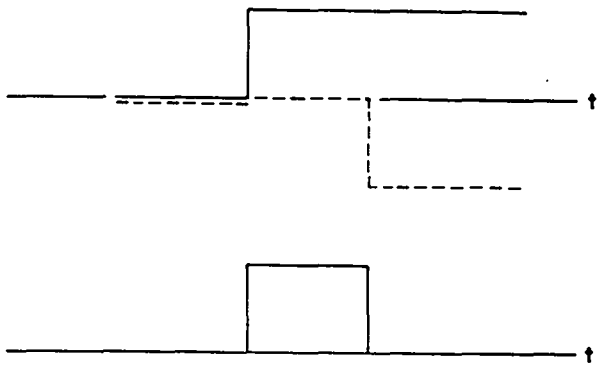

Fig. 16. Two step functions of opposite sign combined to form a square pulse.

A common problem is that of transmitting signals from the detector to a remote receiver. The electrical interference is considered to be in the form of electromagnetic waves incident upon the system and will be represented as a voltage generator acting with an impedance on the system. Probably this impedance will be approximately the so-called characteristic impedance of free space (377 ohms).

It will be seen in Fig. 17 that the most sensitive location for the noise generators is V'_{N1}; hereafter noise generators $V'_{N1}...V'_{Nn}$ will be replaced by an equivalent generator, V_{GL}, of impedance Z_{GL} as shown in the simplified diagram of Fig. 18. The grounding point shown is purely arbitrary, and chosen for convenience rather than because any point exists which can be called ground.

First consider the feed-through signal V_F. Anything that can be done to increase Z_F will reduce this unwanted noise. The most obvious way to do

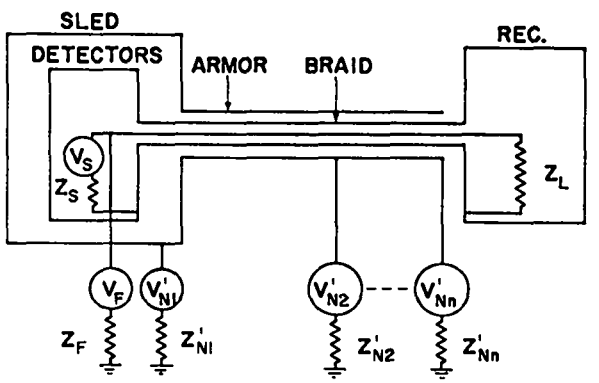

Fig. 17. A transmitting station (sled) and receiving station connected by a doubly shielded cable. The V'_{Ni} are various sources of noise pickup in the system, and V_F is the effective noise signal.

Table II. Cable Response to Various Exciting Functions.

Time	δ Function Input	Step Function Input
To 50% of max	0.291 τ	4.394 τ
To peak	2/3	∞
To 10% of final value	8.5 τ	127 τ
To 5% of final value	13.3 τ	508 τ
To 1% of final value	38.9 τ	12700 τ

this is to increase the thickness of the metal that the waves must penetrate. Table III shows the attenuation for various thicknesses of copper and aluminum. It is also possible to introduce shunt paths for the induced currents and hence transform the single impedance into a "T" attenuator, and, by arranging shielded enclosures inside of enclosures, produce cascaded T-pads. This, however, implies a path for these bypassed currents. In Fig. 18 this path is the braid. Unfortunately, signals flowing in the braid are coupled to the center conductor of the cable and seen by the receiver. This is the reason for the use of a shunt plate (not shown). By connecting the sled shield to ground by a low impedance path which is not tightly coupled to the cables,

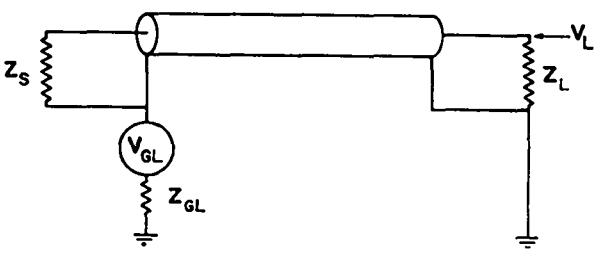

Fig. 18. Idealization for purpose of analysis of transmitting station with impedance Z_S, receiving station with impedance Z_L, and noise generator V_{GL} with impedance Z_{GL}.

Table III. Electromagnetic Attenuation in Aluminum and Copper (to reduce the input wave by 10%)

Frequency (MHz)	Copper (in.)	Aluminum (in.)
1	6×10^{-3}	7.68×10^{-3}
10	1.9×10^{-4}	2.43×10^{-4}
100	6×10^{-4}	7.68×10^{-4}
1000	1.9×10^{-5}	2.43×10^{-5}

a reduction in noise should be achieved.

The noise generator V_{GL} (Fig. 18) acting through impedance Z_{GL} can also be effective in producing noise signals in Z_L at the receiver. To analyze this case, let $V_S = 0$ and $V_F = 0$. The problem is to find the signal developed in the load, V_L, due to the ground-loop voltage, Z_{GL}. By considering the coaxial cable to be a 1:1 transformer with the braid being the primary and the center conductor the secondary, this can be redrawn as in Fig. 19. This transformer is replaced (Fig. 20) by the leakage- and shunt-impedance representations of the transformer; $Z_S = Z_L = Z_O$ (i.e., the line is properly terminated at both ends) and R_C is the resistance of the center conductor, R_S that of the braid or shield.

Before considering the loop equations, it is illuminating to observe the effect of various parameters. If the impedance ωL_s is made very large relative to the other impedances in the i_L current path, the voltage across it is nearly V_{GL}; however, the ideal transformer develops this same voltage thereby forcing the current $i_R \to 0$ and hence $V_L \to 0$. This is the principle of the operation of magnetically loaded lines for ground-loop suppression.

The loop equations are:

$$V_{GL} - i_R 2Z_o - i_R R_C - j\omega i_L L_s - (i_R+i_L)Z_{GL} = 0, \quad (31)$$

$$V_{GL} - i_L R_s - j\omega i_L (L_L+L_s) - (i_R+i_L)Z_{GL} = 0, \quad (32)$$

and

$$V_L = i_R Z_o. \quad (33)$$

After manipulation:

$$V_L = \frac{V_{GL} Z_o (R_s + j\omega L_L)}{Z_{GL}(2Z_o+R_s+R_C+j\omega L_L)+2Z_o[R_s+j\omega(L_L+L_s)]+R_C R_s+j\omega R_C(L_L+L_s)}. \quad (34)$$

Let us consider two special cases.

(A) If the ground-loop noise results from a constant voltage generator, $Z_{GL} \to 0$. Also let $R_C \to 0$, $R_S \to 0$, and $L_L \ll L_s$.

$$V_L = V_{GL} \frac{L_L}{2L_s}. \quad (35)$$

By making $L_s \gg L_L$, $V_L \to 0$. The most practical way

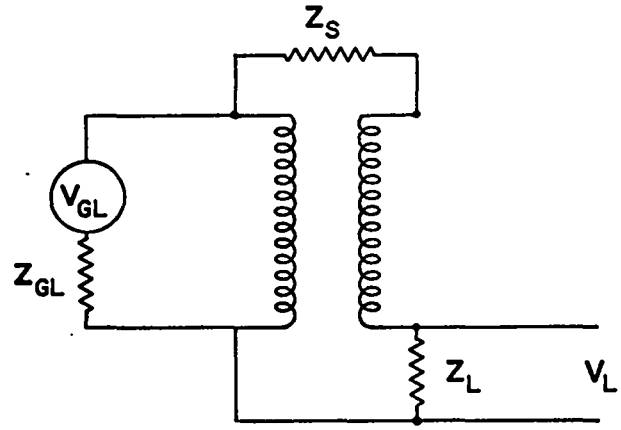

Fig. 19. Reconstruction of a coaxial cable as a 1:1 transformer.

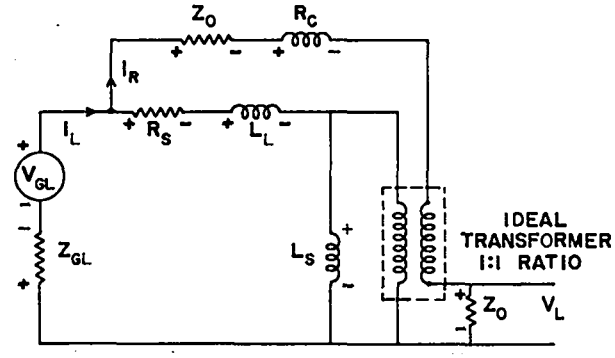

Fig. 20. Replacement for purpose of analysis of 1:1 transformer by elements to represent the leakage inductance and the shunt resistance.

to do this is by winding coaxial cable on a magnetic core. In a test, 28 ft of RG 55 cable were wound on a 3-in. superalloy core. The resulting L_s = 182 mH (at 1 kc), and L_L = 2.24 μH. (The leakage inductance is purely a property of the coaxial cable and is not effected by external influences.) The use of this loaded section reduced 60-cps noise by a factor of more than 1000 in a measured test.

(B) If the ground-loop noise generator is a constant current source, $V_{GL}/Z_{GL} = i_{GL}$, and

$$V_L = \frac{i_{GL} Z_o (R_s + j\omega L_L)}{2Z_o + R_s + R_C + j\omega L_L}$$

for this case, making $L_L \to \infty$ does not help. One must introduce a shunt impedance across the ground-loop noise source (thereby transforming the problem to the preceding case) and then use magnetic loading.

In summary let us consider some previously used techniques from the viewpoint of this model.

(1) Elevation of Cables in a Tray. This is effective because it introduces the extra impedance of an air path between the cables and ground. Since the radiation at this distance is essentially plane, much elevation is not worth the expense. Insulation of 10^4 to 10^5 ohms is satisfactory since this is small compared with 377 ohms. Glass insulators are of doubtful value.

(2) Use of Armored Cables. The armor introduces a shunt path to ground and, hence, tends to increase the coupling impedance.

(3) Cable Bundling. Cables should be bundled to reduce their area in order to minimize induced ground-loop voltages. They should also be crisscrossed to produce positive and negative areas and hence cancel induced currents.

(4) Shunt Paths. Shunt paths are generally useful but not always convenient. If a shunt is used, the previous analysis for ground-loop signals is modified by replacing V_{GL} with $V_{GL}Z_{SH}/(Z_{SH}+Z_{GL})$ and Z_{GL} with $Z_{GL}Z_{SH}/(Z_{GL}+Z_{SH})$ where Z_{SH} is the impedance of the shunt path. Separate shunts on each cable when there are 50 or so involved seems impractical.

(5) Shielding. As many shields within shields as are practical should be used. Shunt paths for the currents should be brought out and taken to ground at the receiving station. The use of very thick shields becomes meaningless unless conductive gasketing materials are used.

Cable Shielding

All signal and control cables are bundled in a wooden trough to keep them off the ground and to isolate them from other conductors which might ground their armor. The metal skin of the recording station has been used as a common grounding point for all coaxial cables and their armor jackets and for the instrument racks within the station. The braid of each coaxial cable is thereafter kept isolated. The armor of one cable is connected to the chamber containing foils and detectors. The "ground" of each detector is provided by the braid on its own coaxial cable only, so there are no ground loops (double grounds) anywhere. The ac power for both recording station and instruments at ground zero is provided by an isolation transformer with neutral of the three-phase four-wire system floating. The whole system consisting of recording station, cables, and detector package is electrically isolated.

Oscilloscopes

Various commercially available oscilloscopes have been used, with little if any modification (except the addition of circuits for intensity control). In some cases oscilloscopes have been mounted on their sides or inverted to bring a cluster of scope tubes into the field of view of one camera.

A practical approach to providing oscilloscopes for streak recording has been to build special units without the many features required for versatility in most commercially available units. These are 10-kV units designed for use in clusters, usually two rows of seven. Diagrams of a scope module for streak recording are given in Figs. 21 and 22. The dc vertical deflection system has response to approximately 8 MHz, symmetrical for ± signals. One-volt input gives full-scale deflection. A step attenuator gain control (max. attenuation 50 to 1), and a time mark input (isolated from the signal input) are provided.

V. SIGNALS

The flux of charged particles into a detector generates a current which passes through a short length (about 10 m) of coaxial cable into a termination at the input of a logarithmic preamplifier. This preamplifier output drives a long coaxial line which terminates at an oscilloscope in the recording station. Typically, 50 sets of detector-amplifier-cable-recorder were used in one experiment, with enough redundancy to allow loss of one detector and line, and additional redundancy in recording channels.

The energy lost by an ionizing particle in a detector corresponds to a definite charge delivered to the output circuit. For a fission fragment with an initial energy of about 85 MeV, a fraction of the energy is lost in emerging from the active deposit of the foil and another fraction is lost in transit through the detector window. The remaining energy, typically 65 MeV, produces electron-ion pairs. We find that a single fission fragment produces a 1.5-mV pulse, 0.1-μsec long, across the 50-ohm resistor at the input to the log amplifier. If we want to limit statistical errors to 1% in an energy range

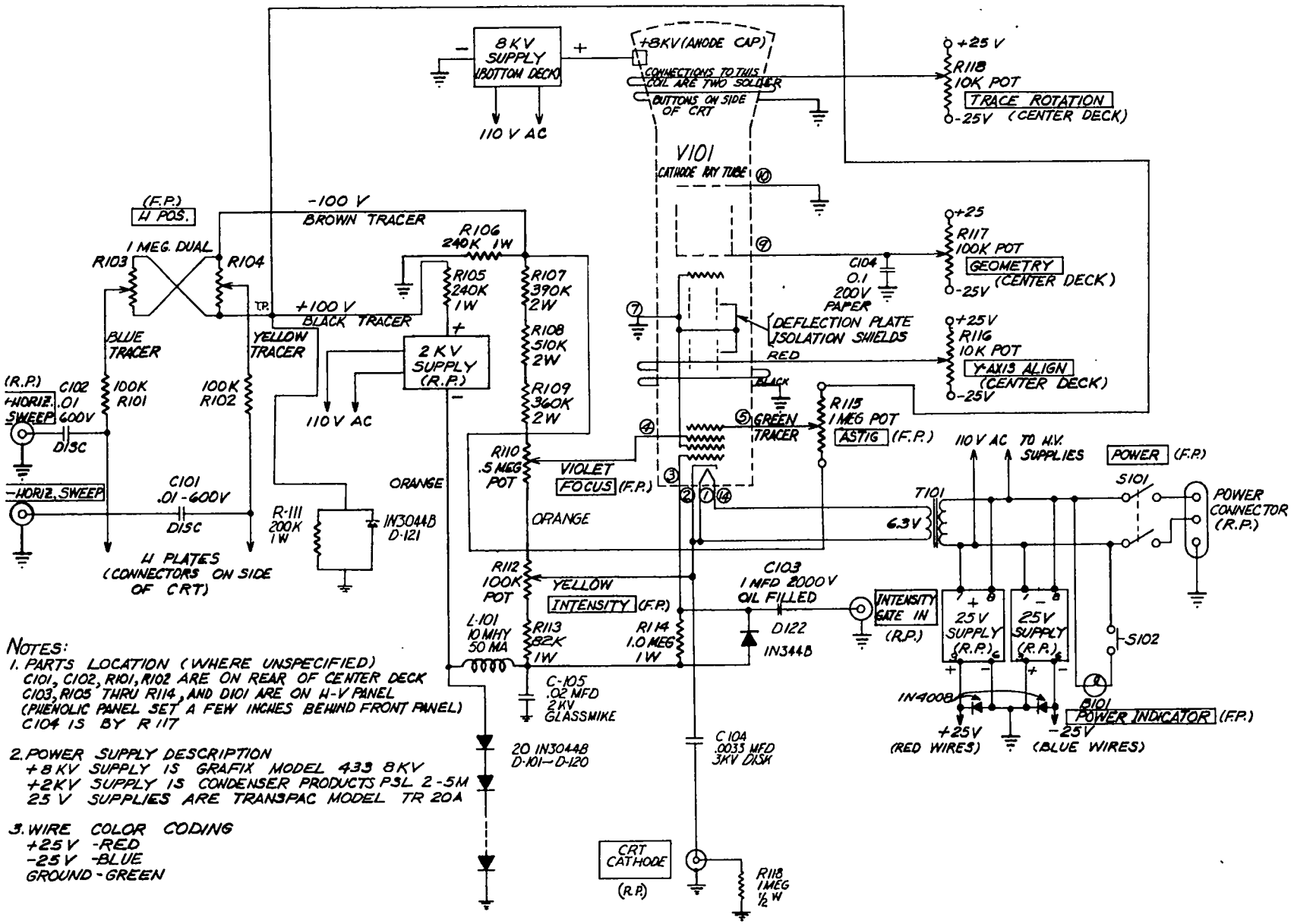

Fig. 21. Oscilloscope module designed for streak recording, less signal preamplifiers.

NOTES:

1. PARTS LOCATION:
   R201 THRU R206 MOUNTED ON SIGNAL ATTENUATOR SWITCH
   R207 THRU R214 AND C201 MOUNTED ON MARKS ATTENUATOR SWITCH
   R215 AND R216 ARE A DUAL POT MOUNTED ON FRONT PANEL
   ALL OTHER COMPONENTS ARE MOUNTED ON THE PLUG-IN AMPLIFIER CARD
2. HEAT SINKS ON ALL TRANSISTORS EXCEPT Q201
3. GROUND SHIELD LEAD ON ALL 2N918 TRANSISTORS

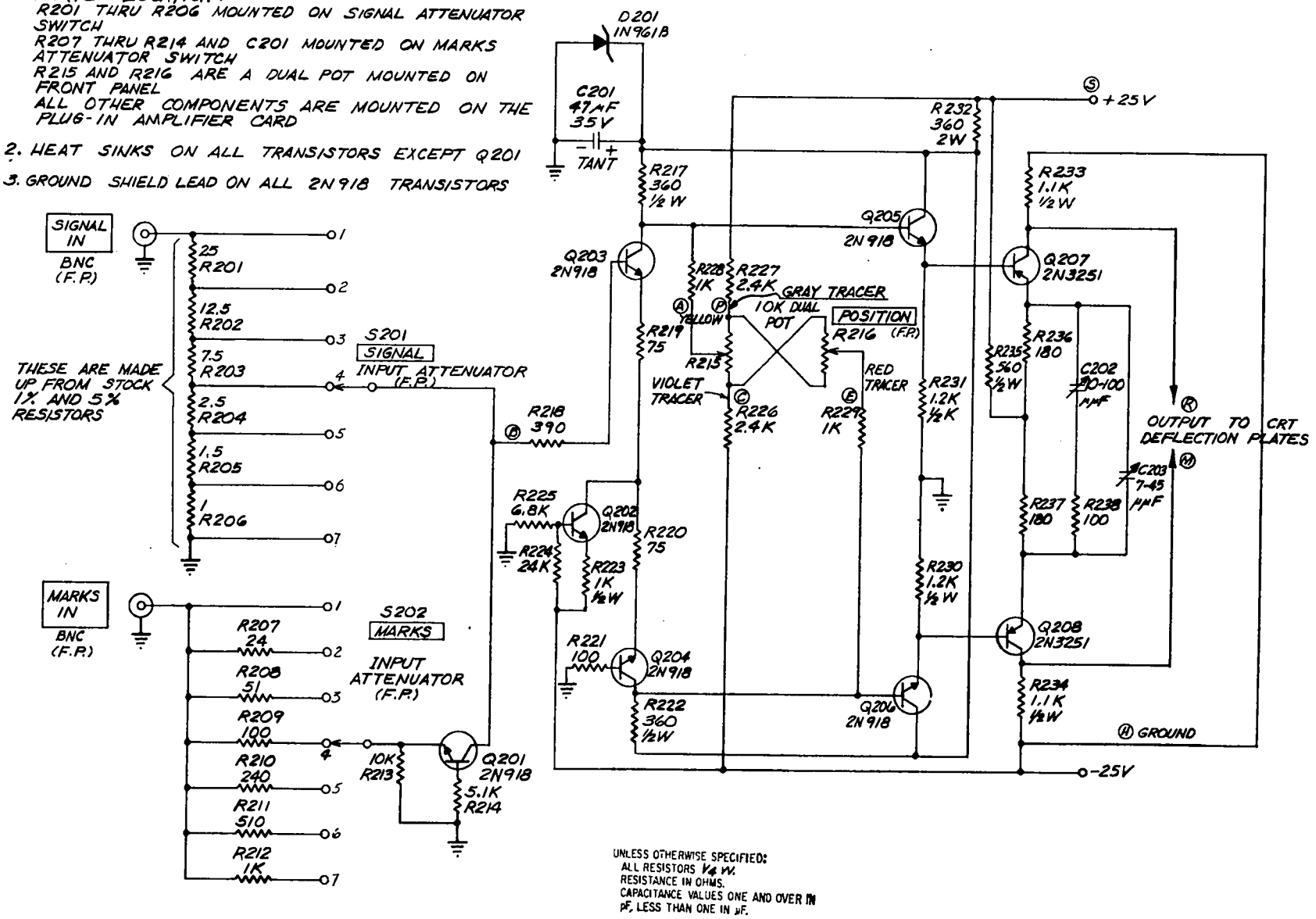

UNLESS OTHERWISE SPECIFIED:
ALL RESISTORS ¼ W.
RESISTANCE IN OHMS.
CAPACITANCE VALUES ONE AND OVER IN pF, LESS THAN ONE IN μF.

Fig. 22. Oscilloscope module designed for streak recording, signal preamplifiers only.

where the resolution is 0.1 μsec, we need a detector output of 15 V; late-model logarithmic preamplifiers have a 10-V output for this input. At energies near 10 eV, where the flux is low anyway, it was necessary to count individual fissions in the valleys between resonances, where cross sections were as small as 0.01 b. It is evident that the working range of a logarithmic preamplifier must be at least four decades; late model high gain units have a five-decade range.

The use of smoothing filters to average the signal over an interval approximating the effective resolving time is a useful expedient for decreasing statistical fluctuation; this also brings a considerable advantage in limiting the writing speed in oscillographic records. Smoothing filters must, however, be used with caution: a peak in the detector signal that is narrow compared to the smoothing time is not represented correctly; the smoothed output of a logarithmic preamplifier does not even give a correct time integral for the signal. Smoothing filters have been constructed as shown in Fig. 23. Using the values

$L = 330\ \mu H$

$R = 1100\ \Omega$

$C = 820\ pf,$

we find

$LC = 0.27\ \mu sec^2$

$RC = 0.90\ \mu sec$

$L/R = 0.30\ \mu sec$

$\omega_o = 0.958\ \mu sec^{-1},$

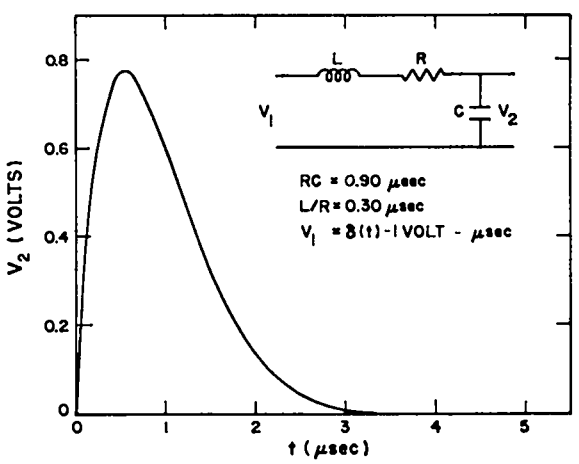

Fig. 23. Signal smoother and its response function to a square wave, one volt x 1 μsec.

and the response of the filter to a delta function with an integral of 1 volt/μsec is

$$V_2 = \frac{e^{-\frac{R}{2L}t}}{\sqrt{LC - \frac{R^2C^2}{4}}} \sin \omega_o t$$

$$= 3.86\ e^{-1.6t} \sin(0.958t).$$

The effect of the filter, whose response is plotted in Fig. 23, is to broaden the peak to 1.4 μsec and to introduce a small amount of undershoot.

VI. DATA RECORDING

To record all the data from one detector we require a system with these characteristics:

Time span	5 msec	for 10-eV low energy limit and 200-m flight path
Time resolution	0.1 μsec	at early time
Dynamic range	5 decades	
Amplitude precision	0.2%	

In the systems used to date, the outputs of logarithmic preamplifiers have been displayed on oscilloscopes and recorded on moving film. A variation of 0.2% in the logarithm of a signal corresponds to a variation of 3% in the signal.

If conventional oscilloscopes are used, the above specifications imply that for an experiment with 50 detectors 1 km of oscilloscope traces must be recorded. This formidable task can be done with various types of moving film cameras.

For early times, where maximum time resolution is required, data have been recorded in "raster" mode: a horizontal drive is applied to the oscilloscope to produce a 20-μsec-long sweep with fast flyback. This cycle is repeated with as little dead time between sweeps as is practical--typically 0.4 μsec. The signal is recorded on film moving in the direction of the signal amplitude deflection (Y direction) so that successive sweeps are separated on the film. Figure 24 shows four signals recorded in this mode on 35-mm film.

For later times, where less resolution is required, data have been recorded in "streak" mode: the motion of the film provides the time base, and the only deflection of the oscilloscope spot is due

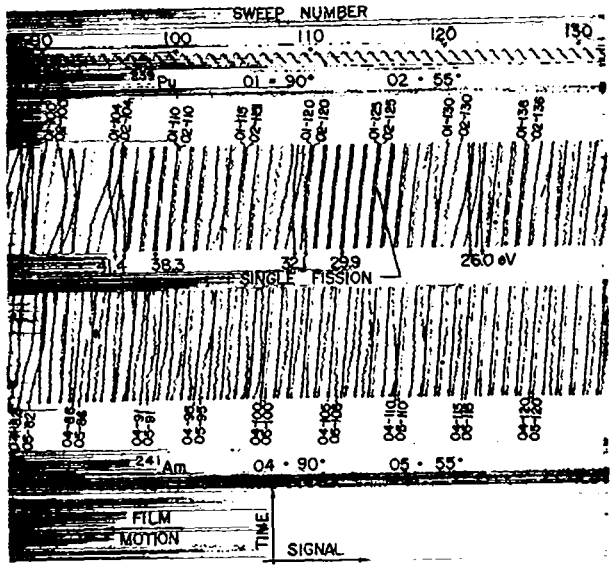

Fig. 24. Four signals recorded in raster mode on 35-mm film; sweep length is 20 μsec, film speed 100 ft/sec. The trace at the top provides both a base line reference and 20-μsec time marks.

to the signal itself; this deflection is at right angles to the film motion. Figure 25 shows signals recorded in this mode on 35-mm film.

The General Radio camera, Type 615AE, long ago considered obsolete for most purposes, has proved

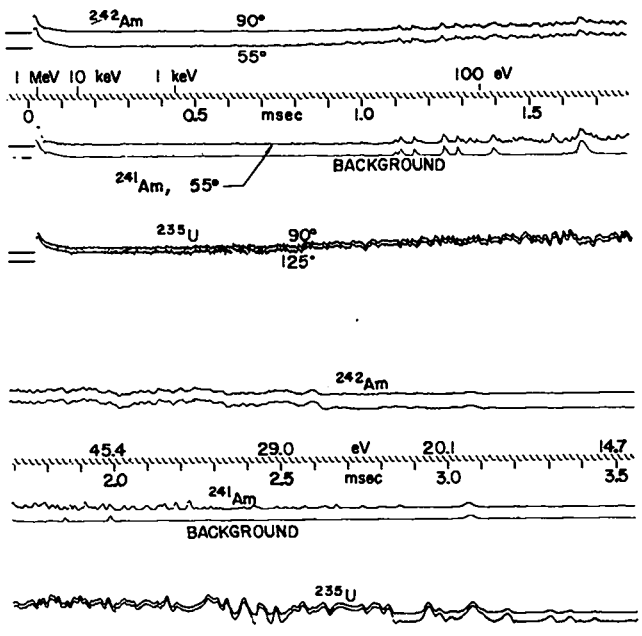

Fig. 25. Six signals recorded in streak mode on 35-mm film; film speed is 100 ft/sec. The third trace from the top provides both a baseline reference and 20-μsec time marks.

useful for making streak and raster records. Use of an object-image ratio of 22 allows recording of signals from several oscilloscopes--usually double beam units--on one piece of film with precision that is limited primarily by the size of the oscilloscope spot. With 250 V ac applied to the series-wound drive motor, a 100-ft-long reel of film attains a speed of 100 ft/sec after half the reel has gone past, and is held at that speed by the action of a centrifugal governor. For either streak or raster records, a reference line is required because the base-line can not be recorded in a separate run. Both time marks and base line are provided by placing in the field of view an additional small oscilloscope whose spot is deflected at right angles to the film transport by a time mark generator; such a reference trace is shown in Figs. 24 and 25.

To get sharp traces on fast moving film, we must use fast decaying cathode ray tube phosphors. The fastest available is known as P-16, whose light output decays to one tenth in 0.12 μsec. The light spectrum from this phosphor peaks, rather inconveniently, at 3850Å so a near-ultraviolet lens is required. The eye is so insensitive to this light that it is easy to burn the screen of a scope. The most suitable film for this application appears to be Eastman 4-X, which is characterized by high speed, small grain size, and relatively small spread with increasing brightness in the width of a trace.

The typical spot diameter produced by an oscilloscope with a P-16 phosphor operating at moderately high intensity is 250μm. For a magnification of 1/22, the image size is 12 μm. The trace on the film is broadened by numerous effects: distortion in the camera lens (typical resolution of a good lens is 50 line pairs/mm), photographic film grain size, and spreading of the image in film processing. The result is a 20-μm spot diameter on the processed film.

If we require 0.1-μsec time resolution at the film, the spot image must move 20 μm in that time, or 200 m/sec relative to the film. The 30 m/sec film speed in the General Radio cameras corresponds to 0.7-μsec resolution for the streak mode. Raster recording with a sweep speed of 0.5 cm/μsec provides 0.1 μsec resolution. A drum camera in streak mode with 250 m/sec film speed also provides the speci-

fied resolution, and, because these records are easier to read, this is the preferred recording mode. In a camera built by Beckman-Whitley, the film is carried on the concave surface of a drum, the objective lens axis is parallel to the axis of rotation; and a mirror directs the light onto the film as indicated in Fig. 26. The drum which rotates in a vacuum, is driven by a series dc motor. A jig facilitates cutting 35-mm film to the right length so that the dead time at the joint is negligible. Drum cameras have been used for recording 14 signals on one 35-mm film, typically with a 30:1 object-image ratio.

Along with the wide range of time and amplitude, an additional recording problem is the wide range of writing speeds. Circuits have been developed to measure the rate of change of the signal and adjust the brightness of the oscilloscope spot so that the recorded trace has a more nearly uniform density; a delay line is required at the scope input to allow time (about 0.1 μsec) for this adjustment.

Systematic adjustment of a large bank of oscilloscopes is facilitated by using:

1. A telescope for viewing a standard signal display to optimize oscilloscope focus;
2. A photometer to indicate standard sweep intensity;
3. A telescope to optimize camera focus for streak or raster recording.

Drum camera focus adjustment has been by cut-and-try. The drum must rotate at operating speed because it stretches radially under rotation, and no scheme for telescopic observation of the image size has proved practical.

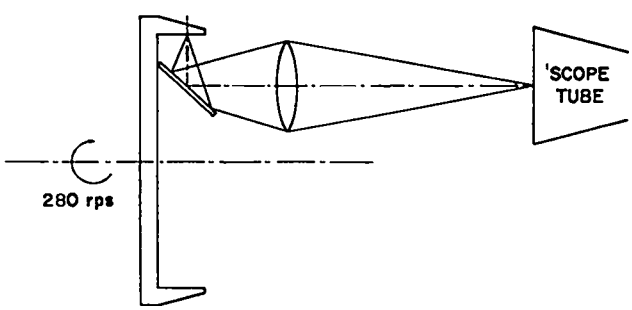

Fig. 26. Schematic of a fast drum camera for recording many scope signals in streak mode on 35-mm film (only one scope is shown). Inside diameter of the drum is 11 in.

A satisfactory lens for the General Radio cameras is the Carl Meyer near-UV, f/2.8, 5 cm. For the drum cameras the Wollensak DuMont CRO f/1.9, 7.5-cm Oscillo-Anastigmat has been used.

The combination of the source burst time, the log preamplifier response, the effect of 1000 ft of coaxial cable, and the recording resolution, each of which approximates 0.1 μsec, gives an overall experimental resolution of 0.2 μsec.

To record a typical resonance on the film at early times requires a variation of one decade in signal amplitude, which amounts to a 1-cm deflection at the scope, and a 2-cm spot travel, to record the peak in 0.1 μsec. The corresponding velocity at the film is 10^4 m/sec--about 50 times faster than the time base. In terms of the image size, this is 5×10^8 trace widths per second. Our experience indicates that this is near the upper limit of writing speed for an f/2.8 lens and P-16 phosphor with 14 kV and Kodak 4x film. A larger aperture lens (with resolution of 50 lines/mm) would have obvious advantages.

The amplitude precision is set by the spot size and deflection sensitivity. To calculate accuracy in signal height, the effect of the log preamplifier must be considered. We designate the scope sensitivity as $\underline{a}$ in volts/cm and the log preamplifier gain as $\underline{b}$ in volts/decade. For our standard preamplifier, the number of decades is equal to $\log v_i$ where v_i is the input in millivolts. Voltage out is then

$$v_o = b \log v_i,$$

signal output in centimeters is

$$h = \frac{b}{a} \log v_i \text{ where } \frac{b}{a} \text{ is in } \frac{\text{cm}}{\text{decade}},$$

and

$$\frac{\Delta v_i}{v_i} = \frac{\ell n\ 10}{b/a} \Delta h.$$

The center of a 20-μ-wide line on film can be determined to 20% of its width, or ±4 μ. Projected back onto the cathode ray tube face, this is equivalent to $\Delta h = \pm 88$ μ. On Parrot and Petrel, typical scope sensitivity was a 4 V/cm. The log amplifiers had b = 2.5 V/decade. Consequently, b/a was 0.6 cm/decade, and $\Delta v_i / v_i$ was about 3%.

Precision also depends upon the reading of the data in relation to the reference trace. This base reference also has a finite thickness, of course, and introduces an additional uncertainty. Generally speaking, the recording system is considered ideally capable of about 5% accuracy.

Table IV summarizes the various measured quantities and their bearing on the precision of the cross section.

VII. CONCLUSIONS

A method for cross-section measurement in the high neutron flux of a nuclear explosion has been developed. This method can provide data with good energy resolution from a few eV to several MeV. It can do so for a small amount of sample material or for short-lived nuclides so radioactive that they contribute impossible backgrounds in the usual laboratory experiments or do not last long enough to allow laboratory measurement.

Table IV. Measured Quantities and Their Contributions to the Percentage of Error in Derived Cross Sections

Target:	
Counts per resolving time	1
Atomic surface density	2
Energy per fission	2
Uncertainty in average energy loss in foil	2
Detector and sample:	
Mount position	1.6
Individual hemisphere dimensions	1
Beam position	2
Detector:	
Pulse height response (Area)	1-2
Uncertainty in average energy loss in window	2
Energy defect uncertainty	2
Electronics and recording:	
Amp-scope calib (log region)	1
Signal reading (log region)	3
Reading reference	3
Overall signal $\delta(n\sigma)$	7

The experiments preceding the Petrel event were mostly involved with developing the method. On Petrel some well-known cross sections were measured as a proof of the method, and some experiments produced new information. On Persimmon many cross sections were measured, most of them new data required in various branches of nuclear technology. Any marked improvements in the actual technique from this point onward will require an increasingly larger effort.

Experiments are planned to exploit further the intense beams available, especially to measure capture cross sections of intense gamma-ray emitters and fission cross sections of highly radioactive nuclides.

VIII. ACKNOWLEDGMENTS

These investigations were made possible by the efforts of hundreds of workers in the Los Alamos Scientific Laboratory and elsewhere. In particular, the continued and effective support of the Los Alamos Field Test Group, whose experience and skill in these unusual experiments was invaluable, is gratefully acknowledged.

REFERENCES

1. J. R. Dunning, G. B. Pegram, G. A. Fink, D. P. Mitchell, and E. Segrè, Phys. Rev. 48, 704 (1935).
2. J. H. Neiler and W. M. Good, "Time of Flight Techniques," in Fast Neutron Physics, Part I, J. B. Marion and J. L. Fowler, Eds., Interscience Publishers, Inc., New York, 1960, p. 509.
3. A. Hemmendinger, Phys. Today (August 1965), 17.
4. B. C. Diven, Proceedings of the International Conference on the Study of Nuclear Structure with Neutrons, M. Néve de Mévergnies, P. Van Assche, and J. Vervier, Eds., North Holland Publishing Co., Amsterdam, Holland, 1966, p. 441.

5-10. Minutes of the Topical Conference on Neutron Cross Section Technology, CONF-660303 (1966), obtainable from: Federal Clearing House for Scientific and Technical Information, National Bureau of Standards, U. S. Department of Commerce, Springfield, VA 22151.

5. Benjamin C. Diven, Paper G-3.
6. E. R. Shunk, W. K. Brown, R. LaBauve, Paper FF-12.
7. D. H. Byers, B. C. Diven, M. G. Silbert, Paper F-5.

8. O. D. Simpson, R. G. Fluharty, M. S. Moore, N. H. Marshall, B. C. Diven, A. Hemmendinger, Paper F-6.

9. D. W. Bergen, M. G. Silbert, R. C. Perisho, Paper F-4.

10. W. K. Brown, D. W. Bergen, J. D. Cramer, Paper FF-11.

11. Los Alamos Scientific Laboratory P-3 and W-8 Staff, Fission Cross Sections from Petrel, report LA-3586 (1966).

12. A. Michaudon, J. Nucl. Energy, 17, 165 (1963).

13. H. A. Sandmeier and G. E. Hanson, Thermal Neutron Spectra from an Underground Nuclear Explosion with Special Consideration of Spectral Modification due to Bomb Debris Motion, Los Alamos Scientific Laboratory report LA-3403 (1965).

14. M. C. Moxon and E. R. Rae, Nucl. Instr. Meth. 24, 445 (1963).

15. A. Hemmendinger, M. G. Silbert, and A. Moat, IEEE Trans. on Nucl. Science, NS-12, 304 (1965).

16. J. S. Lunsford, Rev. Sci. Instr. 36, 461 (1965).

17. A. D. Lewis and F. H. Wells, Millimicrosecond Pulse Techniques, Pergammon Press, 2nd Ed. 1959 Long Island City, N. Y. 11101.

18. W. L. Everitt and G. E. Anner, Communication Engineering, Third Ed., McGraw-Hill Book Co., Inc., New York, 1956.

19. R. L. Wigington and N. S. Nahman, "Transient Analysis of Coaxial Cables Considering Skin Effect," Proc. IRE 45, 166 (Feb. 1957).

20. E. Jahnke and F. Emde, Tables of Functions, Dover Publications, New York, 1945.